# 4

# Fluid Dynamics Analysis of a Space Vehicle Entering the Mars Atmosphere

Antonio Viviani[1] and Giuseppe Pezzella[2]
[1]*Seconda Università degli Studi di Napoli, Aversa*
[2]*Centro Italiano Ricerche Aerospaziali, Capua*
*Italy*

## 1. Introduction

This paper reports the results of design analyses of two Manned Braking Systems (MBS) entering the Mars atmosphere, with the aim of supporting design studies of a planetary entry system. Two lifting body configurations with rounded edge delta-like cross section have been analyzed. The preliminary aerodynamic and aerothermodynamic analyses have considered flight conditions compatible with a manned mission entering the Mars atmosphere. However, neither the mission architecture needed to reach Mars from Earth or neighbour Earth space, nor surface exploration have been addressed.
All the design analyses have been performed at several levels. Indeed, vehicle aerodynamic assessment has been extensively addressed through simplified design approach as, e.g., hypersonic panel methods (HPM); then, a number of fully three-dimensional computational fluid dynamics (CFD) simulations, both with Euler and Navier-Stokes approximations, of the hypersonic flowfield past the entry vehicle have been performed.
The results herein provided have been obtained for a Mars entry scenario compliant with an approach to the red planet both by direct planetary entry and entry after aerobraking (Polishchuk et al., 2006) (Viviani and Pezzella, 2009). These results may be used to provide numerical data for understanding requirements for the human exploration of Mars.

## 2. Computational flowfield analysis

CFD analyses have been performed to assess the aerothermal environment that the MBS experiments during descent, thus evaluating several surface loading distributions (e.g., pressure and heat flux). To this aim, several fully three-dimensional numerical computations, both for perfect and chemically reacting gas approximation, have been performed.
The vehicle configurations, under investigation in this work, are shown in Fig. 1 These lifting bodies feature an aerodynamic configuration with a compact body about 8 [m] long with a rounded edge delta-like cross section (Hanley et al., 1964). A very preliminary internal layout for a crew of four astronauts is also reported in Fig. 1.

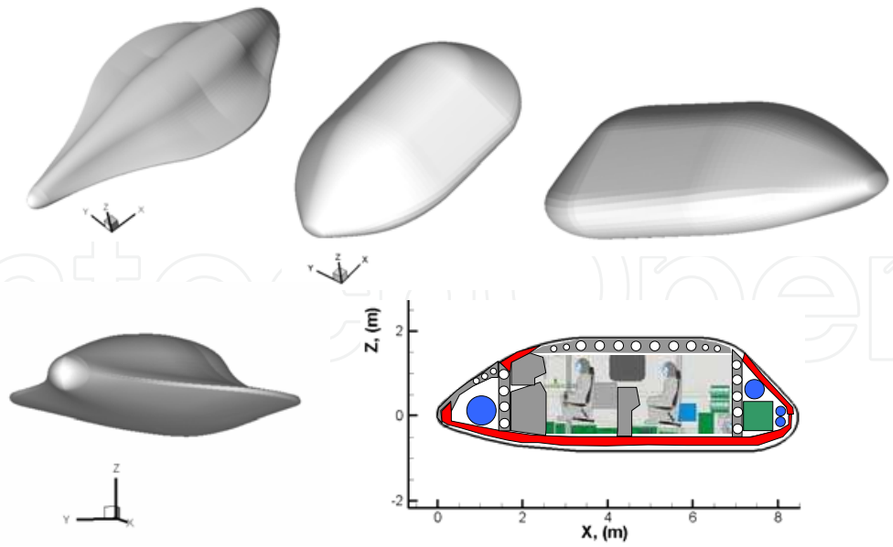


Fig. 1. Vehicle configurations with quotes.

### 2.1 Freestream conditions

The flight scenario considered so far is summarized in Table 1. They refer to entry conditions compatible with a vehicle entering the Mars atmosphere both from a hyperbolic orbit (HO), e.g., direct planetary entry, and an elliptic orbit (EO) e.g., planetary entry after aerobraking (Gupta et al., 1996).

| | | Mach [-] | AoA [deg] | Altitude [km] |
|---|---|---|---|---|
| Perfect Gas | | 10 | 10 | 10.0 |
| | | 15 | 40 | 60.0 |
| | | 22 | 40 | 60.0 |
| | EO PH | 22 | 40 | 44.2 |
| | HO PH | 26 | 40 | 52.1 |
| Reacting Gas | | 10 | 10 | 10.0 |
| | | 10 | 20 | 10.0 |
| | | 10 | 30 | 10.0 |
| | | 10 | 40 | 10.0 |
| EO PH | NCW | 22 | 40 | 44.2 |
| | FCW | 22 | 40 | 44.2 |
| HO PH | NCW | 26 | 40 | 52.1 |
| | FCW | 26 | 40 | 52.1 |

EO PH (Elliptic Orbit Peak Heating)
HO PH (Hyperbolic Orbit Peak Heating)
NCW (Non-Catalytic Wall)
FCW (Fully Catalytic Wall)

Table 1. CFD freestream conditions

Therefore, thirteen CFD numerical simulations have been performed. As one can see, CFD computations (both Euler and Navier-Stokes) have been performed, both in trajectory-based and space-based design approaches (Hanley et al., 1964). Several Mach numbers and

different angles of attack (α) have been investigated and compared each other. The Fluent code together with user defined functions (UDFs), developed in order to simulate mixtures of gas in thermo-chemical non-equilibrium, have been used for CFD computations with a non-equilibrium chemical model suitable for Martian atmosphere (Gupta et al., 1996) (Mack et al., 2008) (Kustova et al., 2009).

For the reacting gas computations, the Martian atmosphere has been considered as a mixture of 95.7% carbon-dioxide, 1.6% Argon and 2.7% nitrogen. The flow has been modelled as a reacting gas mixture of 9 species (Ar, $CO_2$, $N_2$, $O_2$, CO, NO, N, O, C) involved in the chemical reactions of Table 2 (Park et al., 1994) (Anderson, 1989). The reaction mechanism and the related chemical kinetics, taken into account in the present work, are summarized in Table 2, where M is the reacting partner (third body) that can be any of the nine reacting species of the gas mixture.

Non-equilibrium computations have been performed since one of the most challenging problem facing the design of atmospheric entry vehicle is the phenomenon of "real gas behaviour". At hypersonic speeds, the shock wave produced ahead of the vehicle suddenly elevates the gas temperature in the shock layer. So the gas thermal energy may be comparable with the energy associated with a whole range of gas chemical processes such as: molecular vibrational excitation; dissociation of atmospheric molecules into their atomic forms; formation of other chemical species through recombination reactions; and ionisation of both molecular and atomic species (Park et al., 1994).

| Reaction | Third Body M | $A_r$ $[cm^3mol^{-1}s^{-1}]$ | $\beta_r$ | $T_d$ [K] |
|---|---|---|---|---|
| $CO_2 + M \rightarrow CO + O + M$ | ***$CO_2$,CO,$N_2$,$O_2$,NO*** | **6.9x10$^{21}$** | **-1.5** | **63275** |
| | ***Ar*** | **6.9x10$^{20}$** | | |
| | ***C,N,O*** | **1.4x10$^{22}$** | | |
| $CO + M \rightarrow C + O + M$ | ***$CO_2$,CO,$N_2$,$O_2$,NO*** | **2.3x10$^{20}$** | **-1.0** | **129000** |
| | ***Ar*** | **2.3x10$^{19}$** | | |
| | ***C,N,O*** | **3.4x10$^{20}$** | | |
| $N_2 + M \rightarrow N + N + M$ | ***$CO_2$,CO,$N_2$,$O_2$,NO*** | **7.0x10$^{21}$** | **-1.6** | **113200** |
| | ***Ar*** | **7.0x10$^{21}$** | | |
| | ***C,N,O*** | **3.0x10$^{22}$** | | |
| $O_2 + M \rightarrow O + O + M$ | ***$CO_2$,CO,$N_2$,$O_2$,NO*** | **2.0x10$^{21}$** | **-1.5** | **59750** |
| | ***Ar*** | **3.0x10$^{21}$** | | |
| | ***C,N,O*** | **3.0x10$^{22}$** | | |
| $NO + M \rightarrow N + O + M$ | ***$CO_2$,C,N,O,NO*** | **1.1x10$^{17}$** | **0.0** | **75500** |
| | ***Ar*** | **5.0x10$^{15}$** | | |
| | ***CO,$N_2$,$O_2$*** | **5.0x10$^{15}$** | | |
| ***$C_2$+M → C+C+M*** | ***All*** | **2.0x10$^{21}$** | **-1.5** | **59750** |
| ***NCO+M → CO+N+M*** | ***All*** | **6.3x10$^{16}$** | **-0.5** | **24000** |
| $NO + O \rightarrow N + O_2$ | | **8.4x10$^{12}$** | **0.0** | **19450** |
| $N_2 + O \rightarrow NO + N$ | | **6.4x10$^{17}$** | **-1.0** | **38370** |
| $CO + O \rightarrow C + O_2$ | | **3.9x10$^{13}$** | **-0.18** | **69200** |
| $CO_2 + O \rightarrow CO + O_2$ | | **2.1x10$^{13}$** | **0.00** | **27800** |

Table 2. Reactions mechanism and rate parameters (Park et al., 1994).

Therefore, the gas mixture has to be considered in thermal and chemical non-equilibrium. Finally, the CFD analysis of the MBS have been preceded by a code validation phase performed considering the available numerical and experimental data for the Mars Pathfinder probe at entry peak heating conditions, as summarized in (Viviani et al., 2010) (Gnoffo et al., 1998) (Gnoffo et al., 1996) (Mitcheltree et al., 1995).

### 2.2 Numerical results

The aerodynamic analysis of MBS is shown in term of lift ($C_L$), drag ($C_D$) and pitching moment ($C_{My}$) coefficients which are calculated according to Eq. (1) and Eq. (2), respectively.

$$C_i = \frac{F_i}{\frac{1}{2}\rho_\infty v_\infty^2 S_{ref}} \qquad i = L, D \tag{1}$$

$$C_{Mj} = \frac{M_j}{\frac{1}{2}\rho_\infty v_\infty^2 L_{ref} S_{ref}} \qquad j = Y \tag{2}$$

The reference parameters $L_{ref}$ (e.g., longitudinal reference length) and $S_{ref}$ (e.g., reference surface) are the vehicle length (e.g., 8 m) and planform area (e.g., 32 m$^2$). The pitching moment is computed from the vehicle nose (i.e. 0, 0, 0). Engineering based aerodynamic analysis has been extensively performed by using a 3D Panel Methods code developed by CIRA, namely HPM (Viviani and Pezzella, 2009). This tool, at high supersonic and hypersonic speeds, is able to accomplish the aerodynamic and aerothermodynamic analyses of a complex re-entry vehicle configuration by using simplified approaches as local surface inclination methods and approximate boundary-layer methods, respectively. The SIM typical of hypersonics are based on Newtonian, Modified Newtonian, and Prandtl-Mayer theories (Anderson, 1989). Typical surface meshes of the MBS, used for the engineering level computations, are shown in Fig. 2.

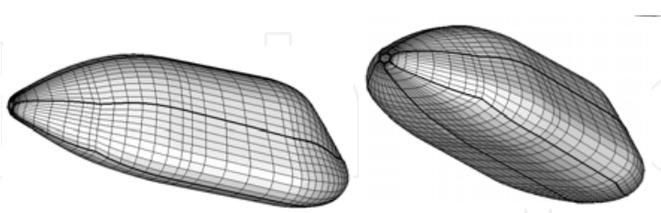

Fig. 2. Example of panel mesh for engineering-based aerodynamic analysis.

MBS aerodynamic results, provided by engineering-based analysis, cover α ranging from 0 to 50 deg. Present CFD computations for the MBS have been carried out on a 3-D multiblock structured grid close to that shown in Fig. 3. The grid consists of about 20 blocks and 900.000 cells (half body). Both computational domains are tailored for the free-stream conditions of Table 1. The distribution of surface grid points has been dictated by the level of resolution desired in various areas of the vehicle such as the stagnation region and the base fillet one, according to the computational scopes. Fig. 3 shows also a close-up view of the 3-D mesh on

the vehicle surface and pitch plane. Grid refinement in strong gradient regions of flowfield has been made through a solution adaptive approach.

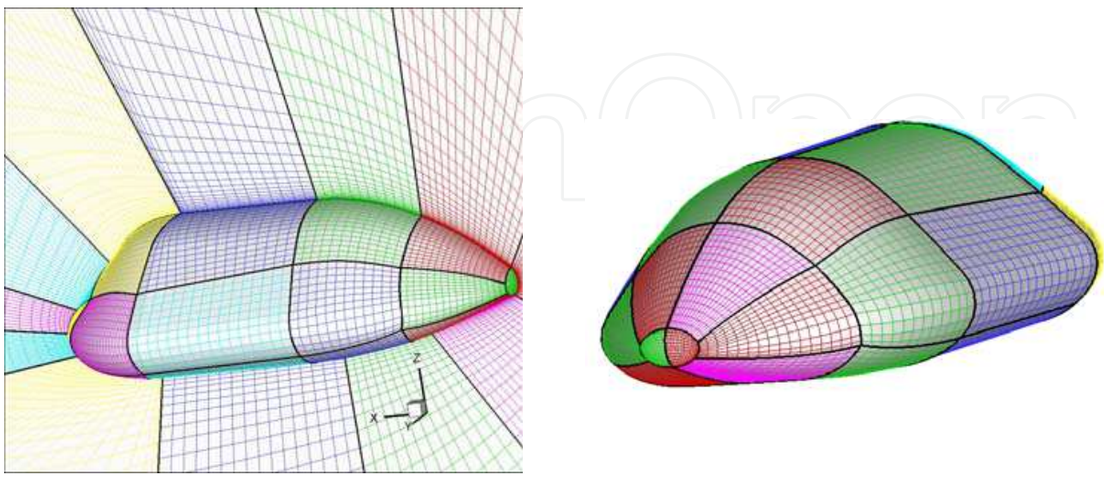

Fig. 3. Example of computational mesh domains for Euler CFD simulations

The preliminary results of CFD simulations performed so far are summarized hereinafter. For example, Fig. 6 shows the static temperature contours on the vehicle symmetry plane and static pressure contours on vehicle surface at $M_\infty$=20 and $\alpha$=20 deg, considering the Mars atmosphere as a reacting gas mixture. As shown, the MBS bow shock structure around the descent vehicle can be appreciated as well.

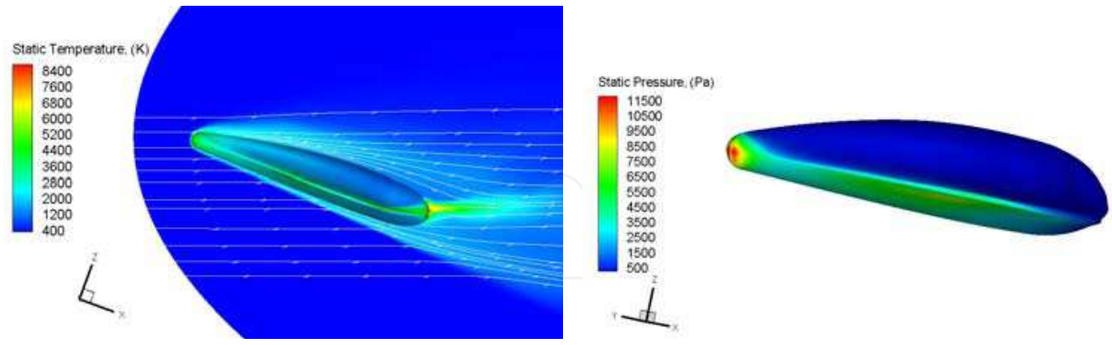


Fig. 4. Results for $M_\infty$=20 and $\alpha$=20 deg. (Left) static temperature field on vehicle symmetry plane; (right) static pressure contour on vehicle surface for non-equilibrium reacting gas

At the same flight conditions, Fig. 5 reports on chemical dissociation of the flow in the shock layer considering the contours of $CO_2$ mass fraction on MBS pitch plane. As a consequence, flow dissociation determines a large density ratio ε across the strong bow shock compared with a flow of the same gas where no dissociation takes place (Viviani and Pezzella, 2009) (Anderson, 1989). This results in a thinner shock layer around the entry vehicle (e.g., lower stand-off distance).

Under conditions where dissociation exists, the aerodynamics of vehicle depends primarily on shock density ratio. In fact, the change of aerodynamic characteristics is the result of change in surface pressure acting on the vehicle forebody (Gnoffo et al., 1998) (Viviani et al., 2010).

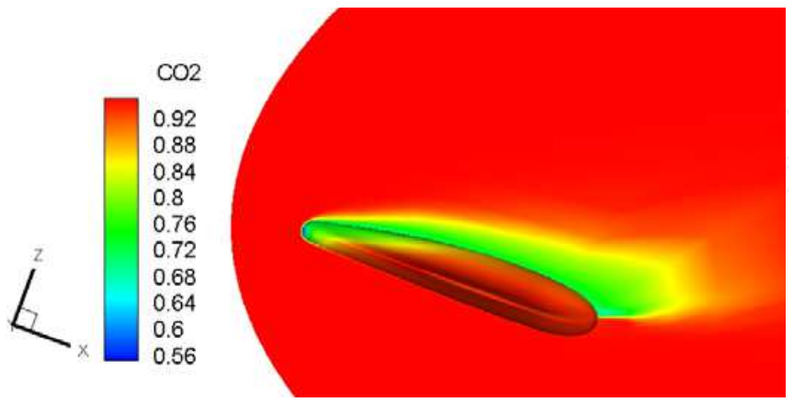


Fig. 5. Results for $M_\infty$=20 and $\alpha$=20 deg. Contours of $CO_2$ mass fraction

Moreover, Fig. 6 shows CFD results for $M_\infty$=21 and $\alpha$=40 deg. The left side reports pressure coefficient contours ($C_p$) on vehicle surface and on two cross sections; whereas on the right $C_p$ contours on vehicle surface and Mach number contours on three cross sections have been shown.

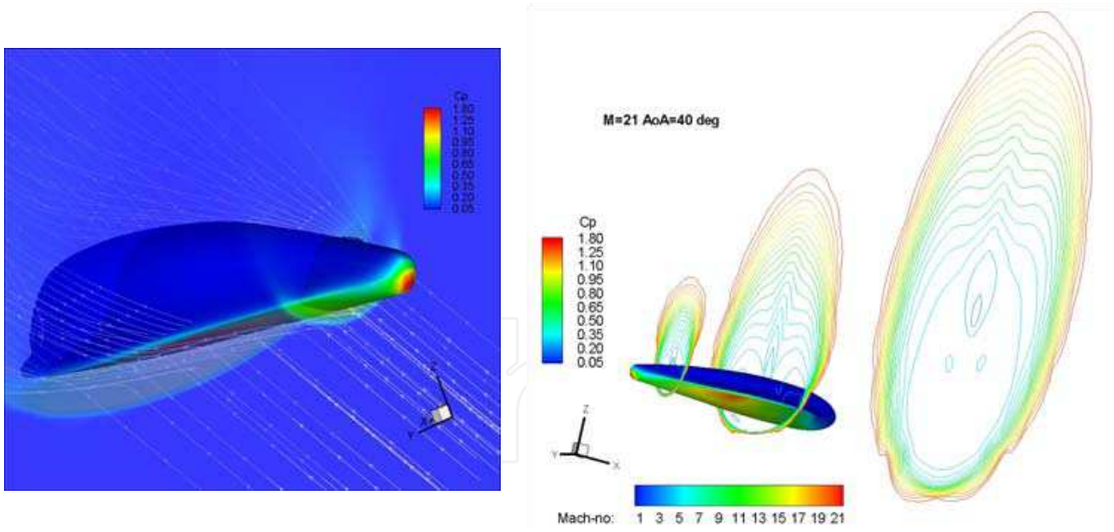


Fig. 6. Results for $M_\infty$=21 and $\alpha$=40 deg. (Left) pressure coefficient contours ($C_p$) on vehicle surface and on two cross sections; (right) $C_p$ contours on vehicle surface and Mach number contours on three cross sections

The curves of lift and drag coefficients are shown in Fig. 7. Those curves collect MBS aerodynamic coefficients compared with available numerical data both for perfect gas and reacting gas approximations, reported in order to highlight accuracy of both numerical and engineering-based results (Viviani et al., 2010).

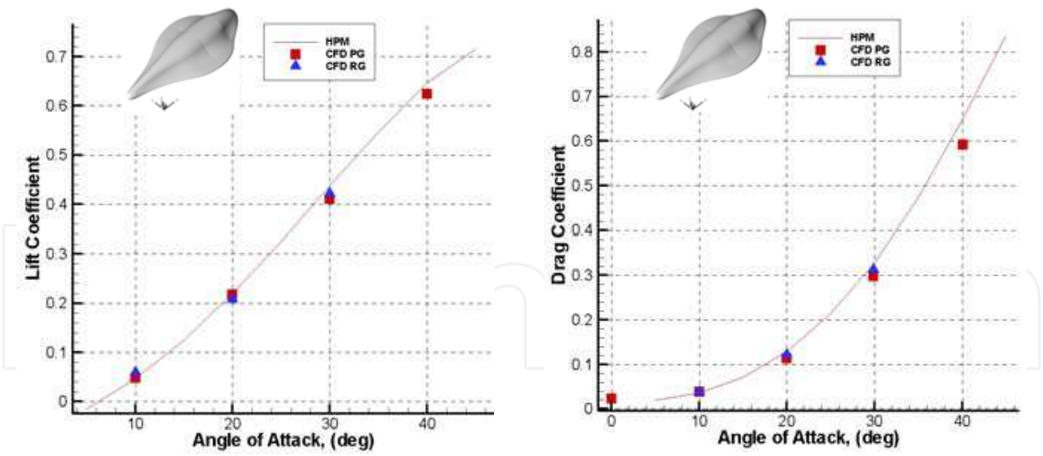


Fig. 7. $C_L$ and $C_D$ versus $\alpha$. Comparison between panel methods and CFD results for perfect and reacting gas approximations.

As one can see, engineering and numerical data compare very well, thus confirming that engineering-based estimations represent reliable preliminary aerodynamics of a Mars entry vehicle. Moreover, real gas effects increase the aerodynamic drag coefficient whereas the lift is only slightly influenced.

As far as CFD results for the second configuration are concerned, Fig. 8 shows the Mach number contour field that takes place around the vehicle when it is flying at the peak heating conditions of entry by EO (e.g., $M_\infty$=22, $\alpha$=40 deg, and H=44.20 km).

In particular, the left side of Fig. 8 shows the Mach contour field on the vehicle pitch plane while at the right side of Fig. 8 gives an idea of the bow shock shape that envelopes the vehicle since the Mach field is reported on three different flowfield cross sections.

As shown, a thin shock layer envelopes the entry vehicle windside with a strong expansion that characterizes the flow at the end of the vehicle.

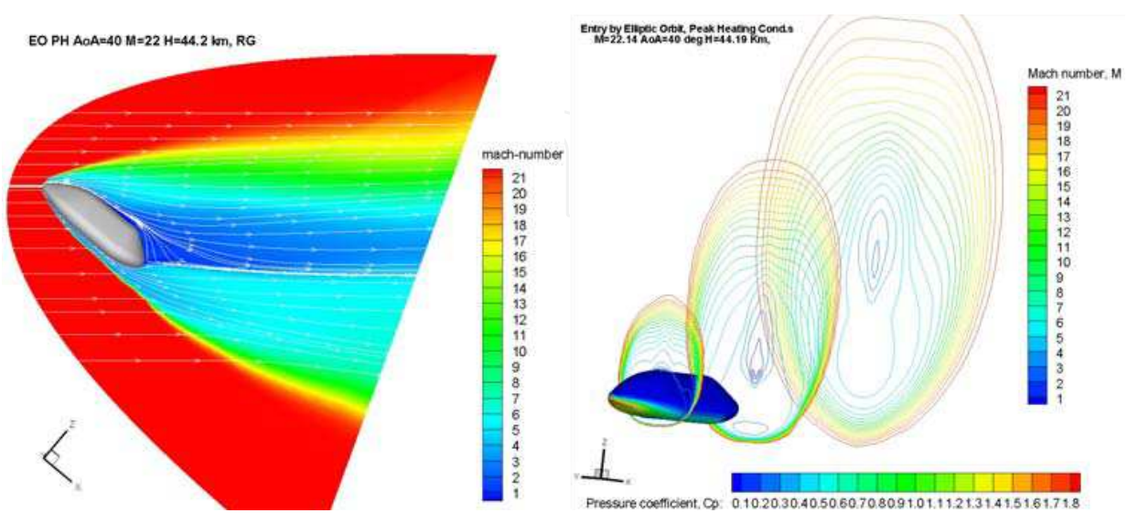


Fig. 8. Mach contours on the vehicle pitch plane and three flowfield cross sections at the EOPH conditions.

The CO mass fraction field around the vehicle for the same freestream conditions is shown in Fig. 9 where some streamtraces colored by Mach number are also reported.

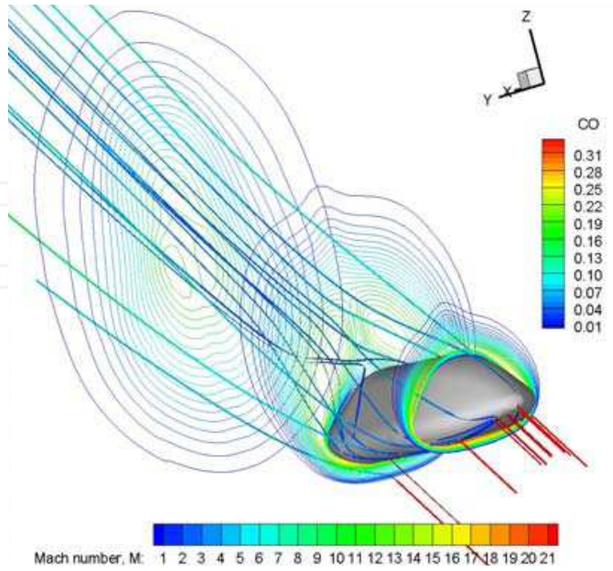


Fig. 9. CO mass fraction at the EOPH conditions on three cross sections with streamtraces colored by Mach number

As shown the CO concentration reaches its maximum value close to the body. Fig. 10 shows the temperature comparison among non-equilibrium flow (right side of pilot) and perfect gas computation, evaluated at three flowfield cross sections (x=1.5 [m], 5.5 [m] and 9.5 [m]). It is clearly evident how real gas phenomena affect the vehicle shock layer, thus confirming all the conclusions highlighted before.

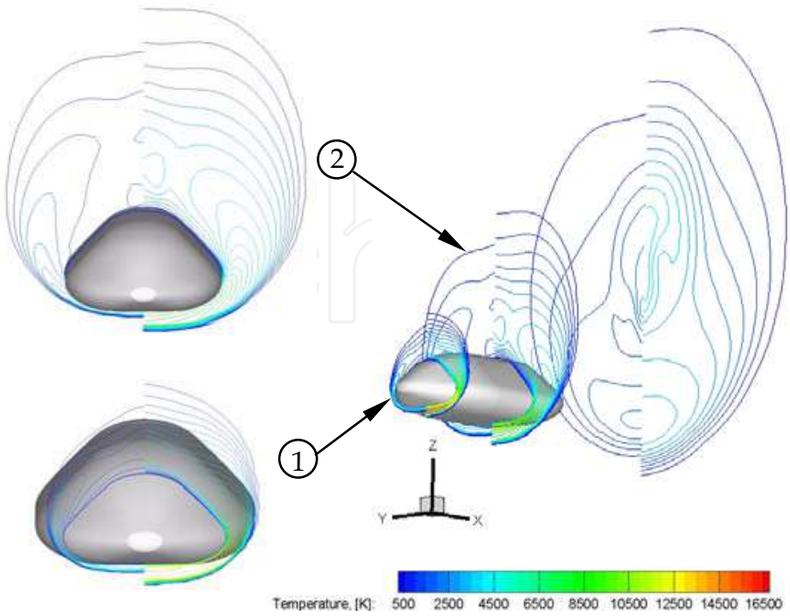


Fig. 10. Temperature comparison between non-equilibrium flow (right side of pilot) and perfect gas computation at x=1.5 [m], 5.5 [m] and 9.5 [m] flowfield cross sections

Finally, the curves of lift, drag, and pitching moment coefficients are shown in Fig. 11.
Real gas effects increase both drag and pitching moment coefficients, whereas the lift is only slightly influenced. Vehicle aerodynamics is also summarized in the table of Fig. 11.

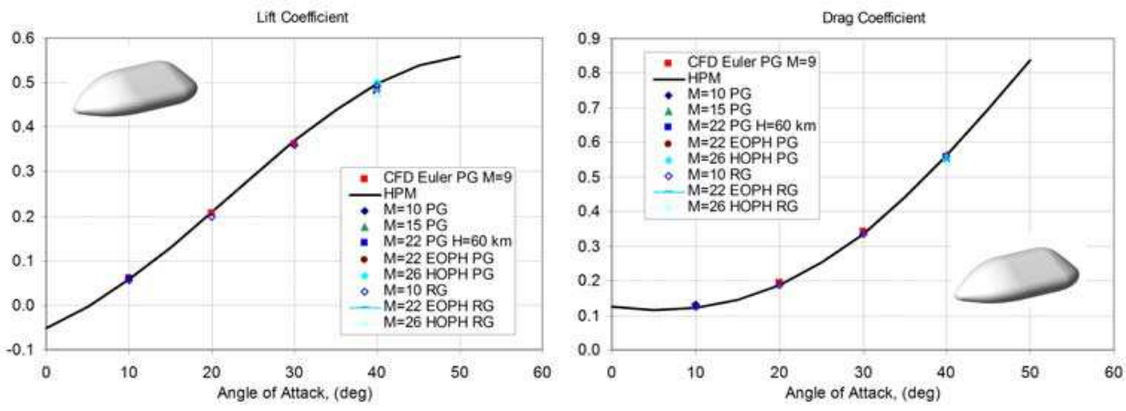


| | | Mach [-] | AoA [deg] | Altitude [km] | CL [-] | CD [-] | CM* [-] |
|---|---|---|---|---|---|---|---|
| Perfect Gas | | 10 | 10 | 10.0 | 0.06150 | 0.13060 | -0.03170 |
| | | 15 | 40 | 60.0 | 0.47830 | 0.55360 | -0.32940 |
| | | 22 | 40 | 60.0 | 0.47930 | 0.55540 | -0.33010 |
| | EO PH | 22 | 40 | 44.2 | 0.48300 | 0.55500 | -0.33200 |
| | HO PH | 26 | 40 | 52.1 | 0.49920 | 0.55930 | -0.34330 |
| Reacting Gas | | 10 | 10 | 10.0 | 0.05710 | 0.12450 | -0.02950 |
| | | 10 | 20 | 10.0 | 0.19940 | 0.18730 | -0.09930 |
| | | 10 | 30 | 10.0 | 0.35970 | 0.33420 | -0.20650 |
| | | 10 | 40 | 10.0 | 0.49340 | 0.56100 | -0.33770 |
| EO PH | NCW | 22 | 40 | 44.2 | 0.48368 | 0.55014 | -0.32980 |
| | FCW | 22 | 40 | 44.2 | 0.48369 | 0.55018 | -0.32990 |
| HO PH | NCW | 26 | 40 | 52.1 | 0.47122 | 0.53627 | -0.32220 |
| | FCW | 26 | 40 | 52.1 | 0.47875 | 0.54536 | -0.32560 |

EO PH (Elliptic Orbit Peak Heating)
HO PH (Hyperbolic Orbit Peak Heating)
NCW (Non-Catalytic Wall)
FCW (Fully Catalytic Wall)
* pole @ vehicle nose

Fig. 11. Lift, Drag and pitching moment coefficients versus α. Comparison between panel methods and CFD results for perfect and non-equilibrium gas computations.

## 3. Conclusion

The paper deals with the flowfield analysis of two braking systems for manned exploration mission to Mars.
A number of fully 3D Navier-Stokes and Euler CFD computations of the hypersonic flowfield past two lifting body vehicles have been performed for several freestream conditions of a proposed Mars entry loading environment. These evaluations have been aimed at carrying out only a preliminary design of the MBS configuration, in compliance with the Phase-A design level.
The range between Mach 2 and Mach 26 has been analyzed, to provide both aerodynamic databases according to both the space-based and trajectory-based design approaches. Numerical results show that real gas effects increase both the aerodynamic drag and pitching moment coefficient, whereas the lift is only slightly influenced.

## 4. References


Anderson, J. D., *Hypersonic and High Temperature Gas Dynamics*, McGraw-Hill Book Company, New York, 1989.

Gnoffo, P., Weilmuenster, K., Braun, R., Cruz, C., *Influence of Sonic-Line Location on Mars Pathfinder Probe Aerothermodynamics*, Journal of Spacecraft and Rockets, vol. 33 No 2, March-April 1996.

Gnoffo, P., Braun, R., Weilmuenster, K., Mitcheltree, R., Engelung, W., Powell, R., *Prediction and Validation of Mars Pathfinder Hypersonic Aerodynamic Data Base*, 7th AIAA/ASME Joint Thermophysics and Heat Transfer Conference. June 15-18, Albuquerque, NM (USA). 1998.

Gupta, R., Lee, K., Scott, C., *Aerothermal Study of Mars Pathfinder Aeroshell*, Journal of Spacecraft and Rockets, vol.33 No 1, Jan.-Feb. 1996.

Hanley, G. M., Lyon, F. J., *The Feasibility of Spacecraft Deceleration by Aerodynamic Braking at the Planet Mars*, Proc. of the 1th AIAA Annual Meeting. Washington, D.C. June 29-July 2, 1964. AIAA-64-479.

Hannemann, V., Mack, A., *Chemical Non Equilibrium Model of the Martian Atmosphere*, Proc. of the 6th European Symposium on Aerothermodynamics for Space Vehicles. Versailles, France. 3-6 Nov. 2008 – ESA SP-659, January 2009.

Kustova, E.V., Nagnibeda, E.A., Shevelev, Y. D., Syzranova, N.G., *Comparison of Non-Equilibrium Supersonic $CO_2$ Flows with Real Gas Effects near a Blunt Body*, Proc. of the 6th European Symposium on Aerothermodynamics for Space Vehicles. Versailles, France. 3-6 Nov. 2008 – ESA SP-659, January 2009.

Mack, A., *CFD Validation for $CO_2$ Reentry Applications*, 2nd Inter. ARA Days. Arcachon, France, 21-23 October 2008. AA-3-2008-37.

Mitcheltree, R. A., Gnoffo, P. A., *Wake Flow about the Mars Pathfinder Entry Vehicle*, Journal of Spacecraft and Rockets, Vol. 32 No 5, Sept.- Oct. 1995.

Polishchuk, G., Pichkhadze, K., Vorontsov, K., Pavela, V., *Proposal on application of Russian technical facilities for International Mars Research Program for 2009–2015*, Acta Astronautica, Vol. 59, pp.113-118. 2006.

Park, C., Howe, J. T., Jaffe, R. L., Candler, G. V., *Review of Chemical-kinetic Problems of Future NASA Missions, II: Mars Entries*, Journal of Thermophysics and Heat Transfer, vol. 8, No 1, pp. 9-23, Jan-Mar 1994.

Viviani, A., Pezzella, G., *Aerodynamic Analysis of a Capsule Vehicle for a Manned Exploration Mission to Mars*. 16th AIAA/DLR/DGLR International Space Planes and Hypersonic Systems and Technologies Conference. Bremen Oct. 2009. AIAA-2009-7386.

Viviani, A., Pezzella, G., Golia, C., *Aerodynamic and thermal design of a space vehicle entering the Mars atmosphere*. The Fifth International Conference on Thermal Engineering Theory and Applications. May 10-14, 2010 Marrakesh. Morocco.

Viviani, A., Pezzella, G., Golia, C., *Aerothermodynamic analysis of a space vehicle for manned exploration missions to Mars*. 27th International Congress of the Aeronautical Sciences. ICAS 2010. Nice, France, 19-24 September 2010.

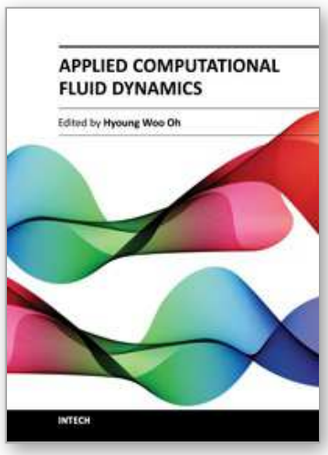


**Applied Computational Fluid Dynamics**

Edited by Prof. Hyoung Woo Oh

ISBN 978-953-51-0271-7
Hard cover, 344 pages
**Publisher** InTech
**Published online** 14, March, 2012
**Published in print edition** March, 2012

This book is served as a reference text to meet the needs of advanced scientists and research engineers who seek for their own computational fluid dynamics (CFD) skills to solve a variety of fluid flow problems. Key Features: - Flow Modeling in Sedimentation Tank, - Greenhouse Environment, - Hypersonic Aerodynamics, - Cooling Systems Design, - Photochemical Reaction Engineering, - Atmospheric Reentry Problem, - Fluid-Structure Interaction (FSI), - Atomization, - Hydraulic Component Design, - Air Conditioning System, - Industrial Applications of CFD



INTECH
open science | open minds

**InTech Europe**
University Campus STeP Ri
Slavka Krautzeka 83/A
51000 Rijeka, Croatia
Phone: +385 (51) 770 447
Fax: +385 (51) 686 166
www.intechopen.com

**InTech China**
Unit 405, Office Block, Hotel Equatorial Shanghai
No.65, Yan An Road (West), Shanghai, 200040, China
中国上海市延安西路65号上海国际贵都大饭店办公楼405单元
Phone: +86-21-62489820
Fax: +86-21-62489821

IntechOpen